Taylor & Francis
Taylor & Francis Group

Science and Technology of Advanced Materials: Methods

ISSN: (Print) (Online) Journal homepage: https://www.tandfonline.com/loi/tstm20

Data-driven estimation of plastic properties of alloys using neighboring indentation test

Ta-Te Chen, Ikumu Watanabe, Dayuan Liu & Kenta Goto

To cite this article: Ta-Te Chen, Ikumu Watanabe, Dayuan Liu & Kenta Goto (2021) Data-driven estimation of plastic properties of alloys using neighboring indentation test, Science and Technology of Advanced Materials: Methods, 1:1, 143-151, DOI: 10.1080/27660400.2021.1959838

To link to this article: https://doi.org/10.1080/27660400.2021.1959838

Published online: 16 Sep 2021.

SCIENCE AND TECHNOLOGY OF ADVANCED MATERIALS: METHODS
2021, VOL. 1, NO. 1, 143–151
https://doi.org/10.1080/27660400.2021.1959838

Data-driven estimation of plastic properties of alloys using neighboring indentation test

Ta-Te Chen [a], Ikumu Watanabe [a,b], Dayuan Liu [a] and Kenta Goto [c]

[a]Graduate School of Science and Technology, University of Tsukuba, Ibaraki, Japan; [b]Research Center for Structural Materials, National Institute for Materials Science, Tsukuba, Ibaraki, Japan; [c]International Center for Young Scientists, National Institute for Materials Science, Tsukuba, Ibaraki, Japan

ABSTRACT

A data-driven estimation method for the plastic properties of alloys was proposed using indentations at neighboring positions. An instrumented indentation test is an efficient approach to measure mechanical properties such as equivalent elastic modulus and hardness. In the mechanical test, subsequent experiments are generally performed apart from existing indentations to avoid the interaction effect caused by the dependency on the deformation history of metal plasticity. In this study, the interaction effect was utilized to estimate the plastic properties, based on the difference of load–depth curves between the first and second indentations at neighboring positions. Using finite element simulations of the neighboring indentation tests, the effective experimental conditions were examined, and response surfaces of the loading curvatures were characterized to determine two material constants of a simple constitutive model of plasticity. Finally, the proposed approach was validated for application to aluminum alloys and stainless steel. It can be also applied to various alloys characterized by different elastic moduli.

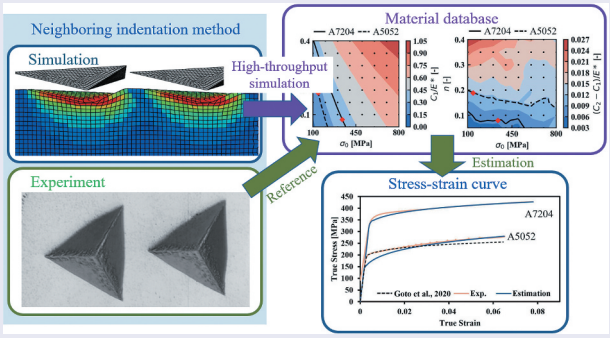

ARTICLE HISTORY
Received 25 March 2021
Revised 11 July 2021
Accepted 21 July 2021

KEYWORDS
Elastic-plastic material; finite element method; mechanical testing; response surface; instrumented indentation test; material database

CLASSIFICATIONS
Data analysis (AI; machine learning; data-driven analysis; descriptor development; structure search/identification)

1. Introduction

Material tests are essential to evaluate material properties, and efficient test methods are required to establish a material database. In structural materials, tensile and compression tests are standard methods for evaluating mechanical properties such as elastic stiffness, yield strength, and work-hardening, in which the stress–strain curve is measured as raw data. Although a simple stress state can be assumed in these material tests, considerable effort is required for specimen preparation and to conduct the tests. In this context, the hardness test, in which the resistance to the imposed plastic deformation is measured on the surface, has been utilized as an efficient approach to estimate the mechanical properties in the industry. It can be used also to evaluate small-scale mechanical properties by controlling a small load; that is, the mechanical properties of a heterogeneous microstructure can be evaluated [1–3]. Using this technology, high-throughput evaluation of microscopic mechanical properties has been conducted to characterize the microscopic heterogeneity [4,5] and obtain massive material data [6].

The instrumented indentation test, depth–sensing indentation test, is an extension of the hardness test [7]. In the instrumented indentation test, the applied load and penetration depth are measured. Based on the resulting relationship between load P and depth h (i.e. the P–h curve) the elastic stiffness and hardness can be estimated [8]. Compared with the uniaxial stress state in tensile or compression tests, an inhomogeneous stress state is produced in the instrumented indentation test. Nevertheless, various estimation approaches for the stress–strain relationship

CONTACT Ikumu Watanabe WATANABE.Ikumu@nims.go.jp Graduate School of Science and Technology, University of Tsukuba, National Institute for Materials Science, 1-2-1 Sengen, Tsukuba, Ibaraki 305-0047, Japan

corresponding to the tensile test have been proposed based on the results of instrumented indentation tests. In this field, it is recognized that a unique stress–strain relationship cannot be estimated from the P–h curve of a single indentation using a standard sharp indenter [9–11]. In this context, a dual–indenter approach and a spherical indenter approach were established. The dual-indenter approach [12–14] using two sharp indenters with different apex angles enables us to determine a unique set of material parameters in a simple constitutive model. The spherical indenter approach [15–17] is based on the nonlinear relationship between the indentation depth and cross-sectional area of the indentation. The above approaches focused only on the P–h curves, whereas Goto et al. [18,19] appended the topography of the indentation impression to the P–h curve for determining the plastic properties.

In these approaches, an indentation test was performed independent of the other tests. Subsequent indentation tests are generally performed at a position apart from the existing indentation impressions to avoid the interactions caused by the dependency of metal plasticity on the deformation history; that is, the interaction between two indentations is sensitive to the plastic properties. It is reported that the residual stress and plastic strain affect the measurement of equivalent elastic modulus and hardness [20–22]. In this study, we focused on the interactions between the existing and subsequent indentation tests. The concept of this proposed approach is to extract the plastic properties from the results of two indentation tests performed at neighboring positions. With this view, finite element simulations were performed to design suitable indentation conditions and draw the response surfaces of the indentation results to determine the material constants of the plastic constitutive model. The response surfaces function as a material database. Finally, the proposed approach was validated in applications to aluminum alloys and stainless steel in which the material constants were read from the response surfaces.

2. Neighboring indentation method

The neighboring indentation method was proposed to estimate the plastic material properties based on the interaction effect between two indentations at neighboring positions.

2.1. Concept

In instrumented indentation tests or hardness tests for alloys, the influence region of the residual stress and plastic deformation can be regarded as approximately two times larger than the size of the indentation impression. Typically, the spacing between the existing and subsequent indentations is set to be large enough to avoid any interaction between them. Following various standards of instrumented indentation testing [23–26], in a simple case of two indentations of the same depth, the second indentation is generally performed at a position that is located at a distance that is five times of the size of the indentation impression away from the first indentation to avoid overlapping plastic strain zones. Phani and Oliver [22] argued that the appropriate indentation spacing is over 10 times the indentation depth to avoid the interaction between indentations for a measurement of elastic modulus and hardness based on experiments and finite element simulations.

The effect of plastic deformation history is expected to result in work-hardening which is a fundamental mechanical behavior in metal plasticity. Therefore, the proposed approach makes active use of the interaction between the first and second indentations. In the approach, the second indentation is performed at a position neighboring the first one.

In instrumented indentation for alloys, the load–depth curve shown in Figure 1 is generally assumed to be a quadratic function:

$$P = Ch^2, \tag{1}$$

where C is the loading curvature. As mentioned in the introduction, additional data on the loading curvature are required to determine a unique set of material constants of the plastic constitutive model, even for the simplest plastic constitutive model [9–11]. In this study, the loading curvature of the first indentation C_1 and the difference of the curvatures $C_2 - C_1$ are chosen as two response variables characterized by the plastic properties. In this approach, the material constants corresponding to the experimental results of indentation curvatures are determined from the

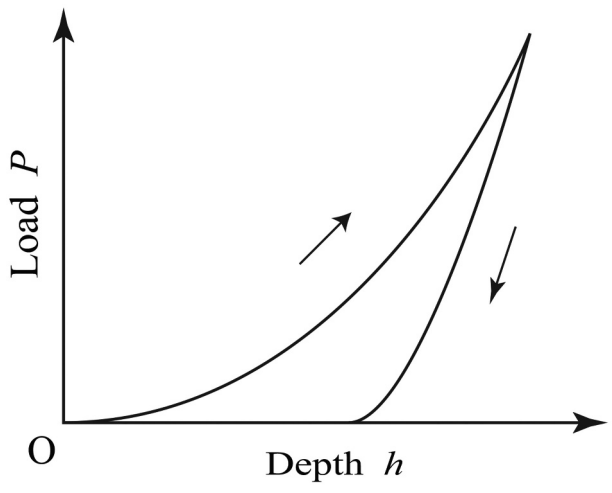

Figure 1. Load–depth curve of the instrumented indentation.

response surfaces, which are prepared using high-throughput simulations based on the finite element method as a material database in advance.

2.2. Constitutive model

An isotropic elastoplastic constitutive model was employed in this study, which is characterized by the St. Venant elasticity and metal plasticity based on the von Mises yield criterion and power-law hardening. The isotropic elasticity includes the Young's modulus E and Poisson's ratio ν. The equivalent stress–strain relationship can be described as follows:

$$\begin{cases} \sigma^* = E^*\varepsilon^* & \text{if } \sigma^* < \sigma_Y \text{ (elasticity)} \\ \sigma^* = K(\varepsilon^*)^n & \text{if } \sigma^* = \sigma_Y \text{ (elastoplasticity)} \end{cases}, \quad (2)$$

where $\sigma^*, \varepsilon^*, E^*, \sigma_Y, K$, and n are the von Mises stress norm, equivalent strain, equivalent elastic modulus, yield stress, plastic coefficient, and work-hardening exponent, respectively. The equivalent strain and equivalent elastic modulus are defined as follows:

$$\varepsilon^* = \sqrt{\frac{2}{3}\mathrm{dev}[\varepsilon] : \mathrm{dev}[\varepsilon]} \quad \text{and} \quad E^* = \frac{3E}{2(1+\nu)},$$

where ε is the strain tensor. In Equation (2), the continuous condition of the stress and strain states at the initial yield stress σ_0 is written as

$$\sigma_0 = K\left(\frac{\sigma_0}{E^*}\right)^n \quad K = \sigma_0\left(\frac{E^*}{\sigma_0}\right)^n. \quad (3)$$

From Equations (2) and (3), the yield strength σ_Y is calculated as a solution to the following equation:

$$\sigma_Y = \sigma_0^{1-n}(\sigma_Y + E^*\xi)^n, \quad (4)$$

where $\xi = \varepsilon^* - \sigma^*/E^*$ is the equivalent plastic strain. Thus, the constitutive model has four independent material parameters: E, ν, σ_0, and n. In this study, ν is assumed to be 0.3 because the Poisson's ratio of alloys has an approximate value of 0.3 at room temperature [27].

2.3. Finite element model

A three-dimensional finite element model was constructed for simulations of neighboring indentation tests, as shown in Figure 2, in which a mirror symmetrical boundary condition was applied to the X-Y plane along the center of the object, and the vertical displacement along the bottom of the finite element model was constrained. The finite element model included 38,181 nodes and 35,994 eight-node hexahedral elements with reduced integration, where the contact area between the indenter and sample was more finely discretized than the other area. The Berkovich indenter was assumed to be a rigid body,

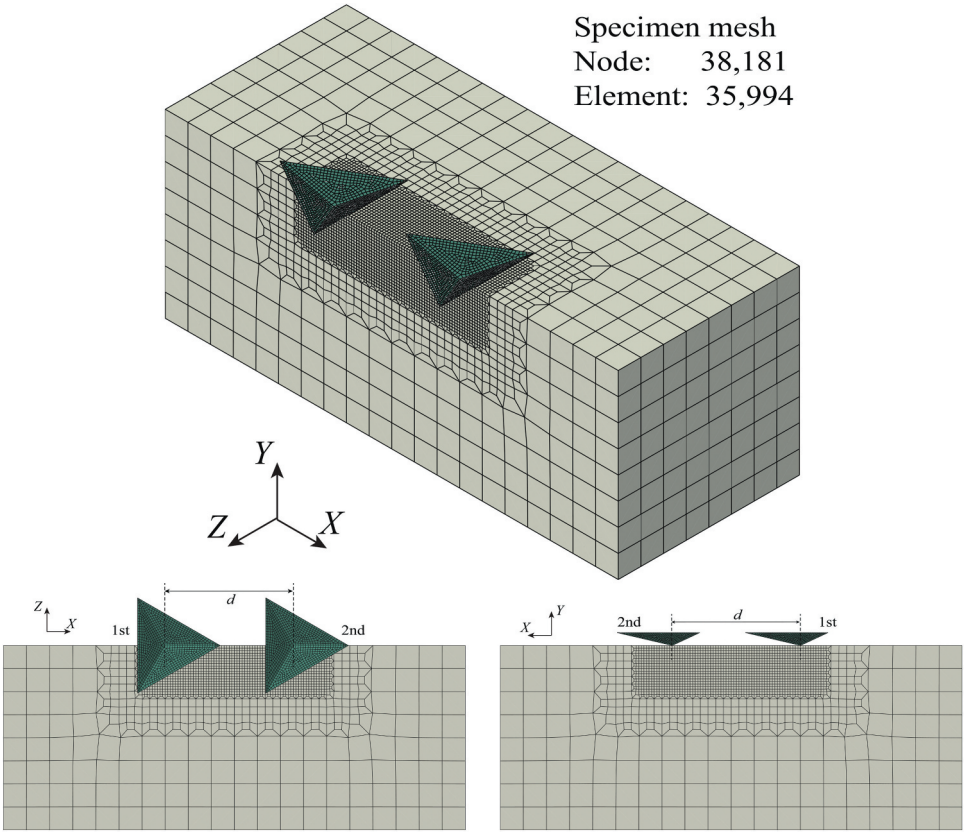

Figure 2. Finite element model of neighboring indentation method.

and the friction between the indenter and sample was not considered in this study. Simulations were performed using displacement control at the top of the indenter and solved as quasi-static boundary value problems with an implicit scheme.

2.4. Numerical examination of indentation conditions

In the proposed approach, the indentation conditions such as the position and depth of the second indentation must be appropriately designed to robustly determine the plastic properties of various alloys. This is because the plastic deformation underneath the indentations depends on both elastic and plastic material properties [22]. In this part, the suitable condition of the neighboring indentation method was numerically examined using finite element simulations.

A series of simulations were performed to investigate the suitable position and depth of the second indentation, where the distance between the first and second indentations d and the maximum depth of the second indentation h_2 for the maximum depth of the first indentation h_1 were examined. h_1 was set to 1 μm for the simulations. The indentation spacing d must be as small as possible, while the maximum depth of the second indentation h_2 must be as large as possible. Therefore, the following two cases were compared:

$$(d/l,\ h_2/h_1) = \begin{cases} (1.2,\ 1.0) & : \text{case(i)} \\ (1.5,\ 1.2) & : \text{case(ii)} \end{cases}, \tag{5}$$

where the spacing and depth were normalized to d/l and h_2/h_1 by the horizontal impression size l and the maximum depth of the first indentation h_1, respectively. Based on the geometry of a triangular pyramidal indenter shown in Figure 3, the impression size l was calculated for a depth h_1 as follows:

$$l = (\tan\theta_1 + \tan\theta_2)h_1 = 6.51h_1, \tag{6}$$

where $(\theta_1,\ \theta_2) = (77.0^\circ,\ 65.3^\circ)$ for the Berkovich indenter. In case (i), a second indentation was performed at the same depth as that of the first indentation. In case (ii), the depth of the second indentation was higher than that of the first indentation, but it was located farther away than in case (i). It is noted that the spacings d were defined to be large enough to avoid the effect of the surface deformation around the impression of the first indentation.

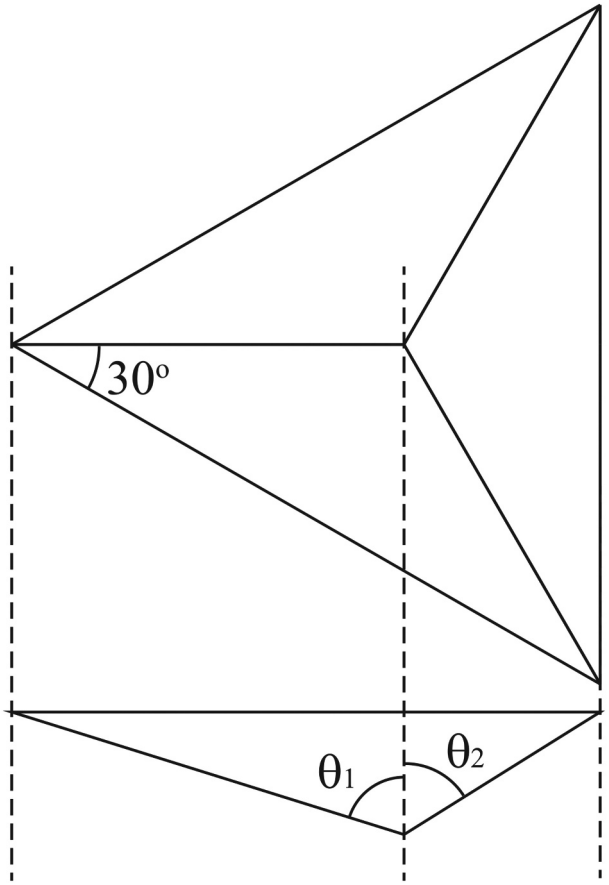

Figure 3. Geometry of a triangular pyramidal indenter.

Results: The response variables C_1 and $C_2 - C_1$ in the two cases of Equation (5) were calculated in the range of $\sigma_0 \in [100\text{MPa},\ 700\text{MPa}]$ and $n \in [0.05, 0.35]$ for two Young's modulus $E =$ 70 GPa and 200 GPa, which are the moduli of aluminum alloy and steel, respectively. The distributions of the response variables are shown in Figures 4 and 5, where the variables were normalized by the equivalent Young's modulus E^*. Based on the calculated mesh data (4×4), the response surfaces were drawn with a bilinear interpolation function. The calculated points were indicated by dots in Figures 4 and 5. In these finite element analyses, 16 calculations were performed for each

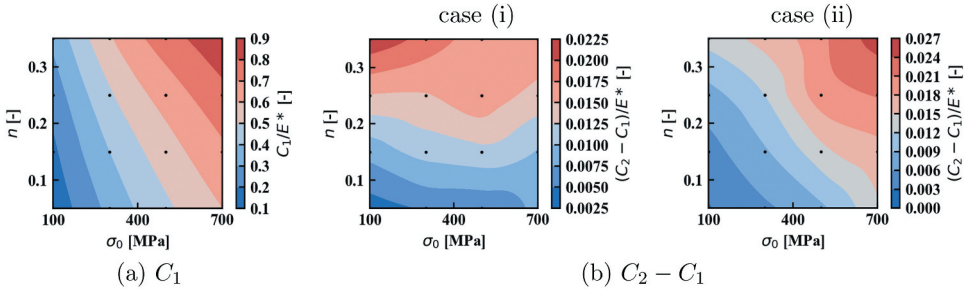

Figure 4. Numerical examination: Response surface of loading curvature in the case of $E = 70$ GPa.

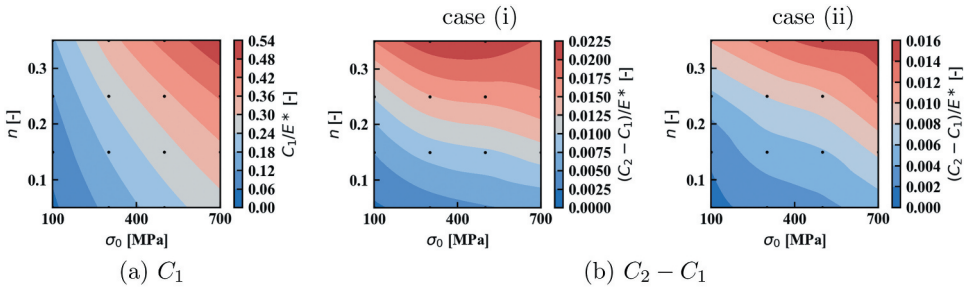

Figure 5. Numerical examination: Response surface of loading curvature in the case of $E = 200$ GPa.

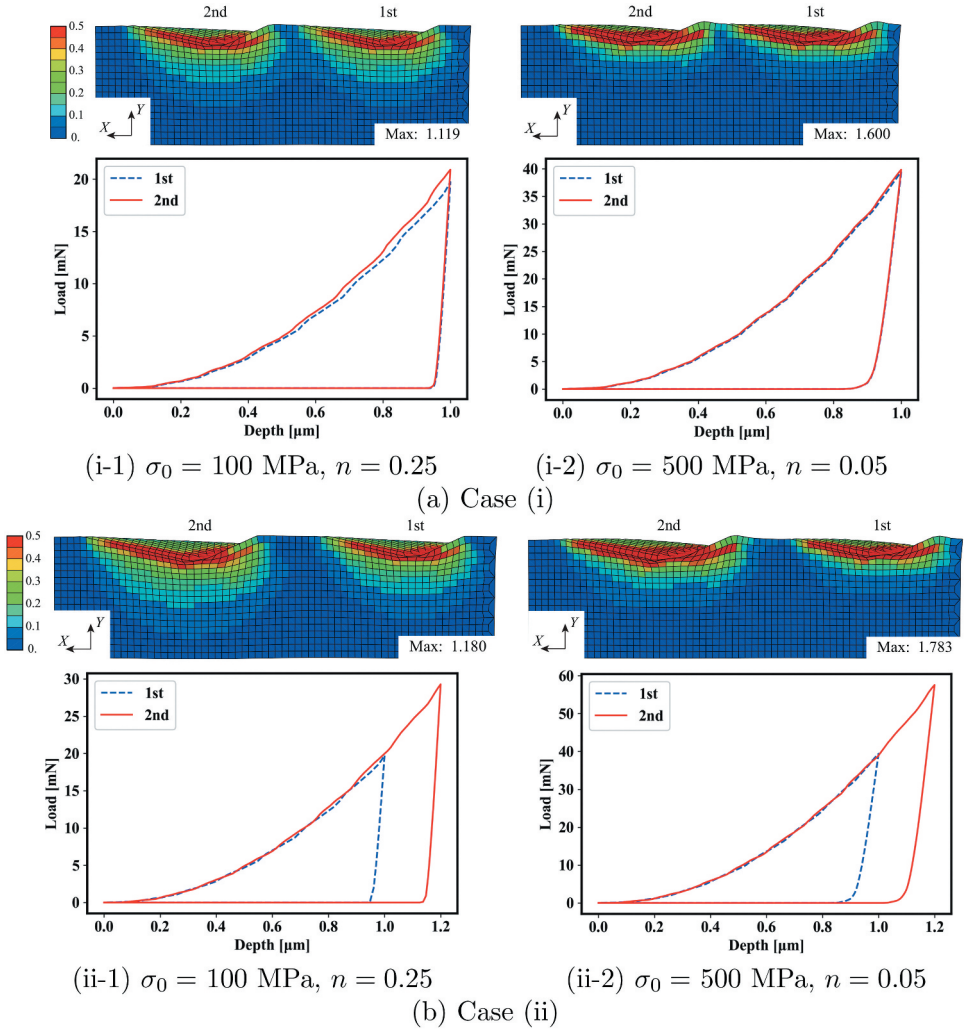

Figure 6. Distribution of equivalent plastic strain under two indentations and its load-depth curves at E=70 GPa.

case. The process required 30 hours because the typical CPU time of a single simulation was approximately 2 hours.

The plastic strain distributions after the second indentation and load–displacement curves of the two indentations are shown in Figure 6 as representative results of finite element simulations for the two sets of material constants at $E =$ 70 GPa. The plastic strain was distributed without a blank in both simulations of case (i); in contrast, in case (ii), the distribution of plastic strain was discontinuous or the overlapping area of plastic strain was very small. As a result, the response variable $C_2 - C_1$ is relatively small in case (ii).

To obtain a unique solution with the neighboring indentation method, the important features of the response surfaces are as follows:

- The response surface is smooth and has a large difference between the maximum and minimum values.

- The two response surfaces have a different tendency.

From the above aspects, the case of $(h_2/h_1,\ d/l) = (1.0,\ 1.2)$, in which the depths of the two indentations were the same, is better for indentation conditions. Moreover, this case is preferable for experiments because of the simple operation of the equipment.

3. Database production

Following the above numerical examination, the response surfaces similar to those in Figures 4 and 5 were recalculated based on the neighboring indentation method to develop a material database to determine a set of material constants for the plastic constitutive model, in which the calculation mesh (8×8) was finer than those of the previous numerical examinations. The resulting response surfaces are shown in Figures 7 and 8. The process required approximately 120 hours to produce one set of response surfaces. The database is applicable to the experimental data following the experimental conditions $(h_2/h_1,\ d/l) = (1.0,\ 1.2)$. Note that the maximum indentation depth $h_1 = h_2$ should be sufficiently large to eliminate potential errors, including those caused by the geometrical error of the indenter, surface roughness of samples, and nanoscopic strengthening mechanism.

4. Validation

The database produced for the neighboring indentation method was validated for application to aluminum alloys and a stainless steel.

4.1. Experimental tests

Instrumented indentation tests were performed at room temperature with a TI900 TriboIndenter (Bruker, USA) using a Berkovich indenter for three samples: A5052 and A7204 aluminum alloys and SUS304 stainless steel. Mechanical polishing was conducted on the sample surface, followed by electrical polishing to remove the residual plastic strains. Considering the maximum load of the equipment, the maximum indentation depths $h_1 = h_2$ were defined as 8.0, 7.5, and 5.3 μm for A5052, A7204, and SUS304, respectively. Using Equation (6), the indentation spacings were set up as 62.5, 58.6, and 41.4 μm for each sample, respectively. The

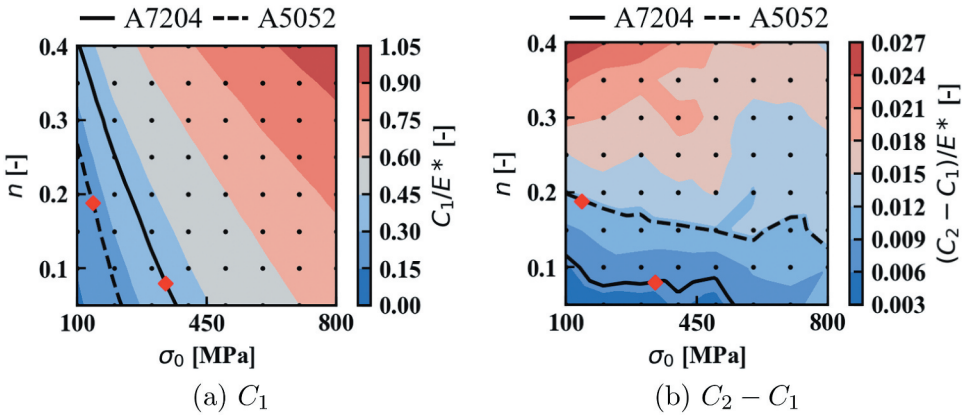

Figure 7. Database: Response surface of loading curvature for $E = 70$ GPa.

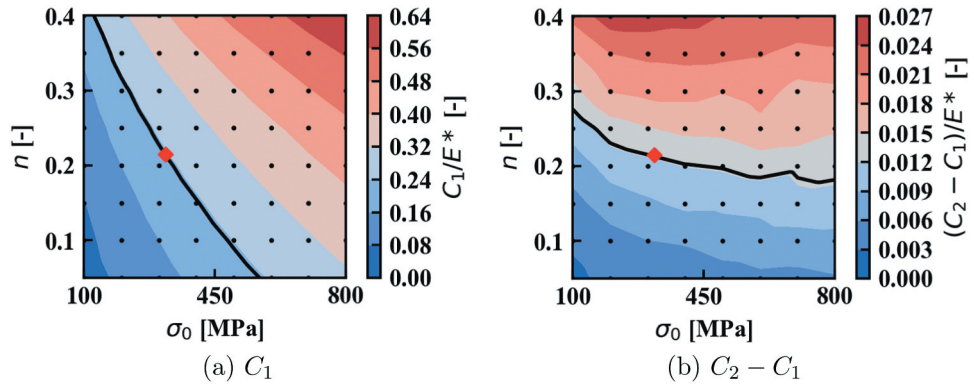

Figure 8. Database: Response surface of loading curvature for $E = 200$ GPa.

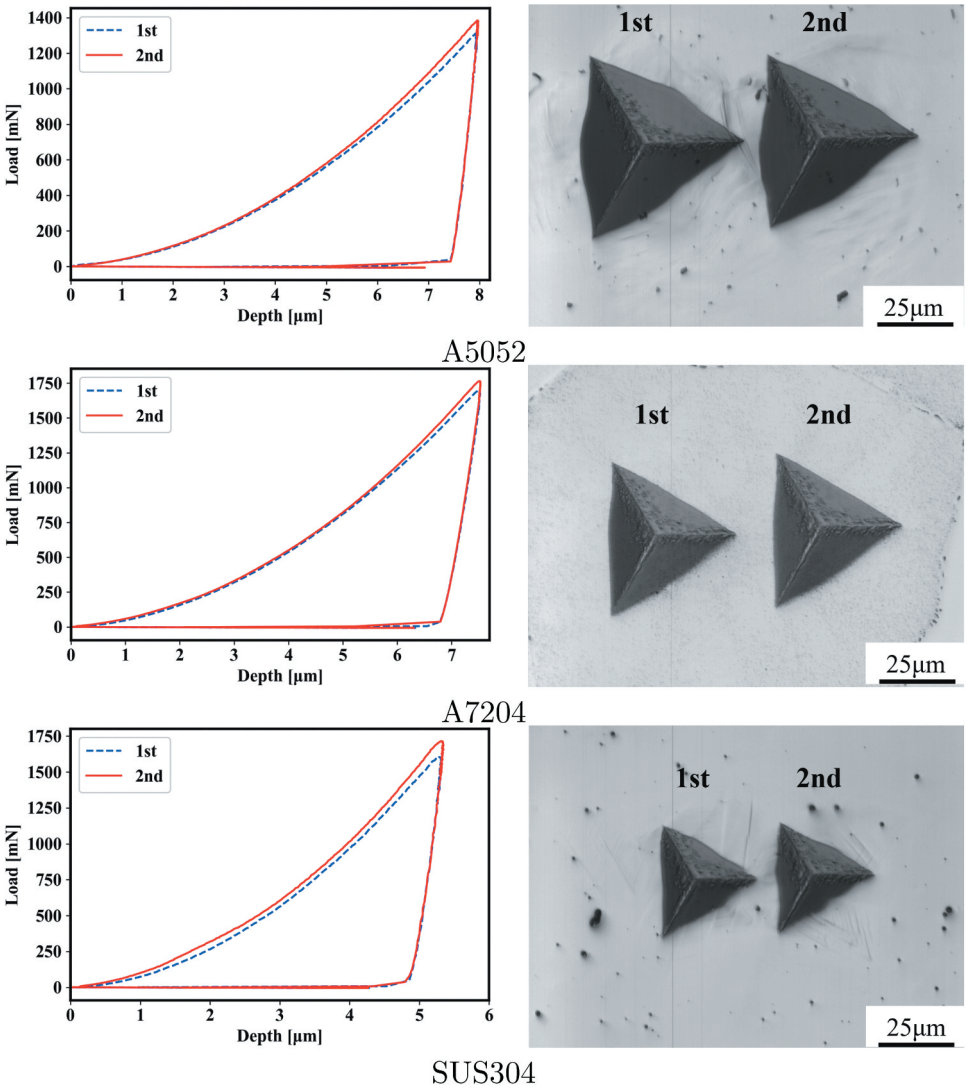

Figure 9. Experimental results: Load–depth curves and indentation impressions of the neighboring indentation test.

loading and unloading rates of the indentation tests were fixed to 0.1 μm/sec. The neighboring indentation tests were performed five times for each sample and the averaged values were used for the estimation to reduce experimental errors.

4.1.1. Results and discussion

The P–h curves and indentation impressions of A5052, A7204, and SUS304 are shown in Figure 9. The grain size of each sample was over 40 μm, and the neighboring indentation tests were performed for a single or few grains with various crystallographic orientations. We so confirmed that the effect of crystallographic anisotropy of the samples on the P–h curves was small in these experiments.

Table 1. Averaged loading curvatures and the deviations obtained from five neighboring indentation tests.

Material	C_1 [GPa]	C_2 [GPa]	$C_2 - C_1$
A5052 aluminum	20.49 ± 0.6	21.42 ± 0.46	0.935 ± 0.466
A7204 aluminum	30.71 ± 0.71	31.24 ± 0.89	0.529 ± 0.239
SUS304 stainless steel	54.03 ± 2.52	56.85 ± 2.93	2.825 ± 1.822

Table 2. Material constants estimated by the neighboring indentation method.

Material	σ_0 [MPa]	n
A5052 Aluminum	142.3	0.187
A7204 Aluminum	338.3	0.008
SUS304 Stainless-steel	317.3	0.215

The averaged loading curvatures of the five neighboring indentation tests and the deviations are shown in Table 1. The experimental values are presented with two curves in Figures 7 and 8. The intersection point indicated by a rhomboid mark is the corresponding material constant. Plastic properties were determined from the set of the two figures, as shown in Table 2. The stress–strain curves of the experimental data and estimation results including another approach [19] are shown in Figure 10. These results agree with the experimental results, especially in aluminum alloys. The power-law hardening used in this study cannot follow the linear hardening behavior shown in Figure 10(b). Even so, the outline of the stress–strain curve is reproduced particularly in the finite strain region.

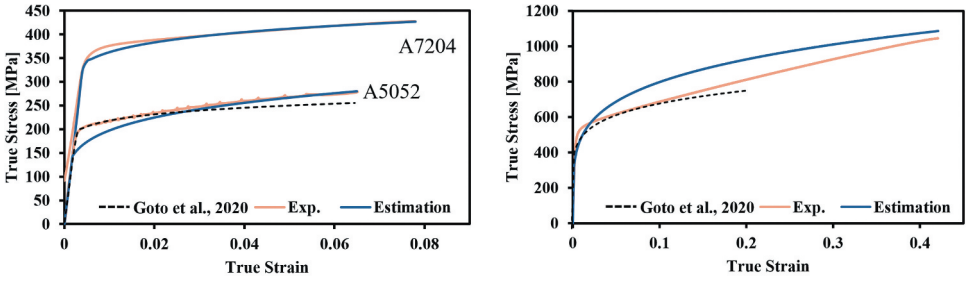

Figure 10. Stress–strain curves estimated by the neighboring indentation method.

As described above, the neighboring indentation method was validated. In this approach, by obtaining the load curvatures C_1 and C_2 under the above-mentioned conditions, the stress–strain curve could be estimated from the response surfaces shown in Figures 7 and 8 in aluminum alloys and steels.

5. Conclusion

A new approach based on instrumented indentation tests was proposed to determine the elastoplastic properties of alloys, in which the interaction effect of indentations at a neighboring position was utilized. Based on the neighboring indentation method, a material database comprising two response surfaces for two material constants of a plastic constitutive model was developed for aluminum alloys and steels using high-throughput simulations based on the finite element method. Using the database, a set of material constants can be determined easily. The produced database was validated by comparison with the corresponding experiments.

Following the proposed concept, a material database can be generated for various alloys with different Young's moduli. This approach is practical because the experiment can be performed using a single standard sharp indenter, and computational simulations can be performed in advance. In addition, it is applicable to high-throughput experiments.

Acknowledgements

The authors wish to acknowledge Ms. Y. Yamamoto, and Ms. E. Nakagawa, National Institute for Materials Science, Dr. Tatsuya Funazuka, Toyama University, and Dr. Y. Nagata and Y. Shinohara, Nippon Steel Co. for their technical support.

Disclosure statement

No potential conflict of interest was reported by the authors.

Funding

This research was financially supported by the Amada Foundation for Metal Work Technology [grant number AF-2018035-C2] and JSPS KAKENHI [grant number 21H01220].

ORCID

Ta-Te Chen http://orcid.org/0000-0002-0553-4736
Ikumu Watanabe http://orcid.org/0000-0002-7693-1675
Kenta Goto http://orcid.org/0000-0002-0102-0658

References

[1] Ruzic J, Emura S, Ji X, et al Mo segregation and distribution in Ti Mo alloy investigated using nanoindentation. Mater Sci Eng A. 2018;718:48–55.
[2] Watanabe I, Sun Z, Kitano H, et al Multiscale analysis of mechanical behavior of multilayer steel structures fabricated by wire and arc additive manufacturing. Sci Tech Adv Mater. 2020;21:461–470.
[3] Matsuno T, Ando R, Yamashita N, et al Analysis of preliminary local hardening close to the ferrite–martensite interface in dual–phase steel by a combination of finite element simulation and nano-indentation test. Int J Mech Sci. 2020;180: PMID 105663.
[4] Hintsala ED, Hangen U, Stauffer DD. High-throughput nanoindentation for statistical and spatial property determination. JOM. 2018;70(4):494–503.
[5] Chen Y, Hintsala E, Li N, et al High-throughput nanomechanical screening of phase-specific and temperature–dependent hardness in AlxFeCrNiMn high-entropy alloys. JOM. 2019;71(10):3368–3377.
[6] Ikeda A, Goto K, Osada T, et al High-throughput mapping method for mechanical properties, oxidation resistance, and phase stability in Ni-based superalloys using composition-graded unidirectional solidified alloys. Scr Mater. 2021;193:91–96.
[7] VanLandingham MR. Review of instrumented indentation. J Res Natl Inst Stand Technol. 2003;108 (4):249–265. PMID 27413609 .
[8] Oliver WC, Pharr GM. An improved technique for determining hardness and elastic modulus using load and displacement sensing indentation experiments. J Mater Res. 1992;7(6):1564–1583.
[9] Cheng Y, Cheng C. Can stress–strain relationships be obtained from indentation curves using conical and pyramidal indenters? J Mater Res. 1999;14 (9):3493–3496.
[10] Tho KK, Swaddiwudhipong S, Liu ZS, et al Uniqueness of reverse analysis from conical indentation tests. J Mater Res. 2004;19(8):2498–2502.
[11] Alkorta J, Martinez-Esnaola JM, Sevillano JG. Absence of one-to-one correspondence between elastoplastic properties and sharp-indentation load–penetration data. J Mater Res. 2005;20(2):432–437.

[12] Futakawa M, Wakui T, Tanabe Y, et al Identification of the constitutive equation by the indentation technique using plural indenters with different apex angles. J Mater Res. 2001;16(8):2283–2292.
[13] Bucaille JL, Stauss S, Felder E, et al Determination of plastic properties of metals by instrumented indentation using different sharp indenters. Acta Mater. 2003;51(6):1663–1678.
[14] Chollacoop N, Dao M, Suresh S. Depth-sensing instrumented indentation with dual sharp indenters. Acta Mater. 2003;51(13):3713–3729.
[15] Taljat B, Zacharia T, Kosel F. New analytical procedure to determine stress–strain curve from spherical indentation data. Int J Solids Struct. 1998;35(33):4411–4426.
[16] Ahn J-H, Kwon D. Derivation of plastic stress–strain relationship from ball indentations: examination of strain definition and pile up effect. J Mater Res. 2001;16(11):3170–3178.
[17] Swadener JG, Taljat B, Pharr GM. Measurement of residual stress by load and depth sensing indentation with spherical indenters. J Mater Res. 2001;16(7):2091–2102.
[18] Goto K, Watanabe I, Ohmura T. Determining suitable parameters for inverse estimation of plastic properties based on indentation marks. Int J Plast. 2019;116:81–90.
[19] Goto K, Watanabe I, Ohmura T. Inverse estimation approach for elastoplastic properties using the load–displacement curve and pile-up topography of a single Berkovich indentation. Mater Des. 2020;194. DOI:10.1016/j.matdes.2020.108925
[20] Wang L, Bei H, Gao YF, et al. Effect of residual stresses on the hardness of bulk metallic glasses. Acta Mater. 2011;59. DOI:10.1016/j.actamat.2011.01.025.
[21] Wang H, Zhang H, Tang D, et al Stress dependence of indentation modulus for carbon fiber in polymer composite. Sci Tech Adv Mater. 2019;20:412–420.
[22] Phani PS, Oliver WC. A critical assessment of the effect of indentation spacing on the measurement of hardness and modulus using instrumented indentation testing. Mater Des. 2019;164. DOI:10.1016/j.matdes.2018.107563
[23] ISO-14577. Metallic materials – instrumented indentation test for hardness and materials parameters. Switzerland: ISO Central Secretariat Geneva; 2002.
[24] ISO-6507-1. Metallic materials. Geneva, Switzerland: Vickers Hardness Test ISO Central Secretariat; 2005.
[25] ASTM E384. Standard test method for Knoop and Vickers hardness of materials. Conshohocken: ASTM International; 2016.
[26] ASTM E. Standard test methods for Vickers hardness and Knoop hardness of metallic materials. Conshohocken: ASTM International; 2017.
[27] Dieter GE. Mechanical Metallurgy. New York: McGraw-Hill; 1986.